Bioorganic Chemistry 114 (2021) 105064

Contents lists available at ScienceDirect

Bioorganic Chemistry

journal homepage: www.elsevier.com/locate/bioorg

Chemical constituents from basidiomycete *Basidioradulum radula* culture medium and their cytotoxic effect on human prostate cancer DU-145 cells

Seung Mok Ryu [a,b,1], Quynh Nhu Nguyen [c,1], Sullim Lee [d], Haeun Kwon [a], Jaeyoung Kwon [e], Hyaemin Lee [a], Sun Lul Kwon [f], Jun Lee [b], Bang Yeon Hwang [g], Joung-han Yim [h], Yuanqiang Guo [i], Jae-Jin Kim [f], Ki Sung Kang [c,*], Dongho Lee [a,*]

[a] Department of Plant Biotechnology, College of Life Sciences and Biotechnology, Korea University, Seoul 02841, Republic of Korea
[b] Herbal Medicine Resources Research Center, Korea Institute of Oriental Medicine, Naju 58245, Republic of Korea
[c] College of Korean Medicine, Gachon University, Seongnam 13120, Republic of Korea
[d] College of Bio-Nano Technology, Gachon University, Seongnam 13120, Republic of Korea
[e] Natural Product Informatics Research Center, Korea Institute of Science and Technology, Gangneung 25451, Republic of Korea
[f] Division of Environmental Science and Ecological Engineering, College of Life Sciences and Biotechnology, Korea University, Seoul 02841, Republic of Korea
[g] College of Pharmacy, Chungbuk National University, Cheongju 28160, Republic of Korea
[h] Korea Polar Research Institute, Korea Ocean Research and Development Institute, Incheon 21990, Republic of Korea
[i] State Key Laboratory of Medicinal Chemical Biology, College of Pharmacy, Tianjin Key Laboratory of Molecular Drug Research, Nankai University, Tianjin 300350, People's Republic of China

ARTICLE INFO

Keywords:
Basidiomycete
Basidioradulum radula
Hyphodermin
DU-145 prostate cancer cell
Cytotoxicity

ABSTRACT

Eight new naphtho[1,2-*c*]furan derivatives (**1**–**8**) along with six known analogues (**9**–**14**) were isolated from culture medium of the basidiomycete *Basidioradulum radula*. The structures of these compounds were identified using spectroscopic analysis, and their absolute configurations were resolved using X-ray diffraction, ECD, and VCD. Compounds **7** and **14** inhibited the cell viability of human prostate cancer DU-145 cells with IC_{50} values of 7.54 ± 0.03 μM and 5.04 ± 0.03 μM, respectively. At 8 μM, compounds **7** and **14** increased the percentage of apoptotic cells and upregulated the protein expression related to the apoptosis caspase pathways in DU-145 cells. Furthermore, the hallmarks of cells undergoing apoptosis, such as chromatin condensation, were also observed at this concentration. However, compound **7** and **14** showed no effect on the proliferation of splenocytes isolated from cyclophosphamide-induce immunosuppressed mice.

1. Introduction

The basidiomycete *Basidioradulum radula* (Fr.) Nobles (syn. *Hyphoderma radula*) is a fungus belonging to the family Schizoporaceae [1]. This strain was first reported in 1967 and is widely distributed in Europe, Australia, North America, and East Asia [2–4]. However, there are few studies reporting the metabolites produced by *B. radula*. Naphtho[1,2-*c*]furan derivatives, hyphodermins A–H, have been isolated from *H. radula* culture medium [5]. Natural and synthetic hyphodermin derivatives exhibit glycogen phosphatase inhibitory activity, and these compounds have been reported to exhibit potential as antiasthmatic, anti-inflammatory, and antidiabetic agents [5–8].

Naphthofuran derivatives such as naphtho[2,3-*b*]furan and naphtho[1,2-*b*]furan derived compounds were reported for their anticancer effect [9–13]. However, very few research have been done to investigate the cytotoxicity effect of naphtho[1,2-*c*]furan derivatives extracted from *B. radula* and its mechanism in human prostate carcinoma cells.

Prostate cancer is one of the most common cause of cancer death in men around the word [14]. Its prognosis is usually poor owing to the asymptomatic early stage in most patients [15]. Current treatments such as surgery and radiotherapy have many disadvantages because of possible metastasis or effects on the patient's quality of life [16]. Moreover, prostate cancer has exhibited emerging resistance to many classes of cytotoxic chemotherapeutics [17]. DU-145 and PC-3 cell lines have high metastasis potential [18,19] and considered as standard cell lines for therapeutic research of prostate cancer [20]. DU-145 is

* Corresponding authors.
E-mail addresses: kkang@gachon.ac.kr (K.S. Kang), dongholee@korea.ac.kr (D. Lee).
[1] These authors contributed equally to this work.

https://doi.org/10.1016/j.bioorg.2021.105064
Received 13 January 2021; Received in revised form 12 May 2021; Accepted 2 June 2021
Available online 5 June 2021

considered as androgen-independent [21]. Androgen-independent prostate cancer cells are resistant to chemotherapy drugs induced apoptotic caspases [22]. Furthermore, DU-145 is Bax-negative and p53 mutant cell line [23]. Therefore, DU-145 cells is a suitable model to investigate the cytotoxicity effect of chemotherapy agents against human prostate carcinoma.

In the search to discover biologically active compounds from fungal strains [24,25], eight new naphtho[1,2-*c*]furan derivatives (**1**–**8**) (Fig. 1), in addition to six known compounds (**9**–**14**), were isolated from culture medium of the basidiomycete *B. radula*. The chemical structures of these isolated compounds were identified, and they were evaluated for cytotoxic effects on DU-145 cells.

2. Results and discussion

Compound **1** was isolated as a white amorphous powder. Its elemental composition was determined as $C_{15}H_{16}O_4$ by HRESIMS analysis. The ^{1}H NMR spectral data exhibited the presence of a germinal dimethyl group [δ_H 1.43 (3H, s, CH_3-4) and 1.47 (3H, s, CH_3-4)], a methoxyl group [δ_H 3.79 (3H, s, OCH_3-10)], two methylene groups [δ_H 2.84 (1H, ddd, J = 17.7, 7.8, 5.3 Hz, H-2), 2.75 (1H, ddd, J = 17.7, 9.2, 5.1 Hz, H-2), 2.13 (1H, ddd, J = 14.2, 9.2, 5.2 Hz, H-3), and 2.06 (1H, ddd, J = 13.6, 7.9, 5.1 Hz, H-3)], an oxymethine group [δ_H 6.69 (1H, s, H-10)], and two aromatic methine groups [δ_H 7.72 (1H, d, J = 8.1 Hz, H-5) and 7.98 (1H, d, J = 8.1 Hz, H-6)] (Table 1). The ^{13}C NMR spectral data exhibited 15 carbon signals assigned to two carbonyl carbons, two dimethyl carbons, one methoxyl carbon, two methylene carbons, three methine carbons including an oxymethine, and five additional quaternary carbons (Table 2). The 1D NMR data obtained for **1** were consistent with those of hyphodermin B (**9**) [7], a known naphtho[1,2-*c*]furan derivative, apart from the presence of an additional methoxy group [δ_H 3.79 (3H, s, OCH_3-10); δ_C 59.0 (OCH_3-10)], which was identified by the HMBC cross peak of OCH_3-10/C-10 (δ_C 104.8) (Fig. 2).

The absolute configuration at the C-10 position of **1** was determined from the comparison between calculated and experimental ECD spectra. The results exhibited that the calculated ECD spectrum of the 10*S* model matched closely with the experimental ECD spectrum, suggesting the absolute configuration of **1** was 10*S* (Fig. 3). Consequently, the new compound **1** was established as shown and has been assigned the trivial name hyphodermin I.

Compound **2** was isolated as a white amorphous powder. The elemental composition of **2** was identified to be $C_{15}H_{16}O_5$ based on the HRESIMS analysis, which was 16 Da more than that of **1**, indicating the presence of an additional hydroxyl group. The 1D NMR data of **2** were similar to those of **1**, except for the absence of a methylene signal of **1** (H-2) and the presence of an oxymethine signal in **2** [δ_H 4.71 (1H, dd, J = 13.9, 5.6 Hz, H-2)] (Tables 1 and 2). In the COSY spectrum of **2**, the oxymethine signal showed a correlation to the methylene signals [δ_H 2.37 (1H, dd, J = 13.2, 5.8 Hz, H-3) and 2.08 (1H, t, J = 13.5 Hz, H-3)] and the HMBC cross peaks of H-2/C-1 (δ_C 198.4), C-3 (δ_C 45.6), C-4 (δ_C 36.2), and C-8a (δ_C 125.4) (Fig. 2) indicated that the oxymethine group in **2** was located at the C-2 position. In addition, the IR spectrum showed an OH stretch at 3493 cm^{-1}. These results exhibited that **2** contained a hydroxyl group at the C-2 position.

Compound **3** was also obtained as a white amorphous powder. Based on the HRESIMS analysis, the elemental composition of **3** was assigned as $C_{15}H_{16}O_5$, which is the same as that of **2**. Detailed analysis of the NMR data of **3** and a comparison with the data of **2** indicated that the planar structure of these compounds was the same. However, the optical rotations of the two compounds showed they possess opposite signs [−165.3 (*c* 0.01, MeOH) in **3** and +166.1 (*c* 0.01, MeOH) in **2**], suggesting these compounds are stereoisomers.

The stereochemistry of **2** and **3**, including the absolute configuration, was determined by analyzing X-ray, ECD, and VCD data. When compound **2** was dissolved in $CHCl_3$ and then dried slowly at 25 °C, colorless needlelike crystals were formed (Supporting Information S56). Thus, using single-crystal X-ray diffraction analysis (Cu Kα), the 3D structure of **2** was confirmed and its absolute configuration [a Flack parameter of 0.07(4)] was determined (Fig. 4). Furthermore, the calculated ECD and VCD spectra of the 2*S*,10*S* and 2*S*,10*R* isomers were in good agreement with the experimental values of **2** and **3**, respectively (Figs. 3 and 5). Therefore, as shown, the structures of the new compounds **2** and **3** were elucidated to be hyphodermin J and isohyphodermin J, respectively.

Compound **4** was obtained as a brown oil and was assigned the elemental composition $C_{15}H_{14}O_5$ based on the HRESIMS analysis. The ^{1}H and ^{13}C NMR data of **4** were in accordance with those of **2** and **3**, except for the presence of a $\Delta^{2(3)}$ double bond [δ_H 6.29 (1H, s, H-3), δ_C 145.2 (C-2), and δ_C 127.1 (C-3)] (Tables 1 and 2), which were deduced based on the HMBC cross peaks of H-3/C-1 (δ_C 179.8), C-2 (δ_C 145.2), C-4 (δ_C 38.5), C-4a (δ_C 157.9), and $(CH_3)_2$–4 (δ_C 30.4 and 30.3) (Fig. 2). The absolute stereochemistry of **4** was established by comparing its calculated and experimental ECD spectra (Fig. 3), thus confirming its 10*S* configuration. Therefore, the structure of the new compound **4**, designated hyphodermin K, was determined as shown.

Compound **5** was isolated as a brown oil, and its elemental composition was assigned as $C_{14}H_{12}O_5$ by HRESIMS analysis. Detailed analysis of the 1D NMR data exhibited that **5** was similar to **4** (Tables 1 and 2) with the only difference in **5** being the absence of a methoxy group at C-10. Furthermore, this result was supported by MS and 2D NMR data (Fig. 2). In solution, **5** exhibited mutarotation due to the hemiacetal group at C-10 [26,27], which was supported by the optical rotation, ECD spectrum, Chiral HPLC analysis, and acetylation reaction (Supporting Information S32–S35). Therefore, the structure of the new compound **5**, designated as hyphodermin L, was established as shown.

Compounds **6** and **7** were isolated as white amorphous powders and had molecular formulas of $C_{15}H_{13}IO_4$ and $C_{14}H_{11}IO_4$, respectively, based on the HRESIMS analysis. Detailed analysis of the 1D and 2D NMR data indicated that the structures of **6** and **7** were similar to those of **4** and **5**, respectively. However, the unusual up-field chemical shifts of C-2 (δ_C 101.5 in **6** and δ_C 100.7 in **7**) suggested that **6** and **7** have a heavy atom at the C-2 position. Considering the molecular formulae of **6** and **7**, it can be concluded that these compounds have an iodine atom at the C-2 position, which was supported by the ESIMS/MS fragment peaks, *m/z* 258 $[M+H-I]^+$ and 226 $[M+H-I-OCH_3]^+$ in **6**, and *m/z* 244

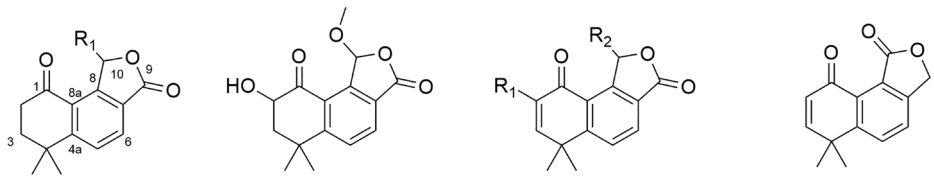

1 (10*S*), R_1 = OCH_3

2 (2*S*, 10*S*)
3 (2*S*, 10*R*)

4 (10*S*), R_1 = OH, R_2 = OCH_3
5 R_1 = OH, R_2 = OH
6 (10*S*), R_1 = I, R_2 = OCH_3
7 (10*S*), R_1 = I, R_2 = OH

8

Fig. 1. Chemical structures of isolated new compounds (**1**–**8**) from *B. radula* culture medium.

Table 1
^{1}H NMR spectroscopic data (500 MHz) of compounds **1**–**8** in $CDCl_3$.

Position	**1**	**2**	**3**	**4**	**5**	**6**	**7**	**8**
	δ_H (*J* in Hz)	δ_H (*J* in Hz)	δ_H (*J* in Hz)	δ_H (*J* in Hz)	δ_H (*J* in Hz)	δ_H (*J* in Hz)	δ_H (*J* in Hz)	δ_H (*J* in Hz)
2	2.84, ddd (17.7, 7.8, 5.3) 2.75, ddd (17.7, 9.2, 5.1)	4.71, dd (13.9, 5.6)	4.56, dd (14.0, 5.5)					6.45, d (10.5)
3	2.13, ddd (14.2, 9.2, 5.2) 2.06, ddd (13.6, 7.9, 5.1)	2.37, dd (13.2, 5.8) 2.08, t (13.5)	2.32, dd (13.1, 5.5) 2.16, t (13.6)	6.29, s	6.38, s	7.75, s	7.84, s	6.86, d (10.5)
5	7.72, d (8.1)	7.72, d (8.1)	7.76, d (8.1)	7.88, d (8.1)	7.89, d (8.1)	7.80, d (8.1)	7.83, d (8.1)	7.88, d (8.1)
6	7.98, d (8.1)	8.02, d (8.1)	8.05, d (8.1)	8.07, d (8.1)	8.11, d (8.1)	8.07, d (8.1)	8.13, d (8.1)	7.65, d (8.1)
9								5.28, s
10	6.69, s	6.75, s	6.52, s	6.78, s	7.09, s	6.78, s	7.08, s	
4-$(CH_3)_2$	1.47, s 1.43, s	1.52, s 1.52, s	1.52, s 1.52, s	1.58, s 1.57, s	1.60, s 1.60, s	1.58, s 1.57, s	1.61, s 1.61, s	1.53, s 1.53, s
10-OCH_3	3.79, s	3.77, s	3.83, s	3.83, s		3.85, s		

Table 2
^{13}C NMR spectroscopic data (125 MHz) of compounds **1**–**8** in $CDCl_3$.

Position	**1**	**2**	**3**	**4**	**5**	**6**	**7**	**8**
	δ_C, Type	δ_C, Type	δ_C, Type	δ_C, Type	δ_C, Type	δ_C, Type	δ_C, Type	δ_C, Type
1	196.9, CO	198.4, CO	197.5, CO	179.8, CO	181.1, CO	177.9, CO	179.8, CO	182.8, CO
2	35.4, CH_2	70.5, CH	70.2, CH	145.2, C	145.2, C	101.5, C	100.7, C	127.6, CH
3	36.5, CH_2	45.6, CH_2	43.7, CH_2	127.1, CH	128.7, CH	165.1, CH	166.6, CH	154.9, CH
4	34.9, C	36.2, C	36.1, C	38.5, C	38.8, C	43.1, C	43.4, C	38.2, C
4a	159.4, C	159.0, C	159.5, C	157.9, C	158.2, C	156.1, C	156.5, C	152.1, C
5	129.7, CH	130.2, CH	130.5, CH	130.3, CH	130.1, CH	130.1, CH	129.9, CH	132.4, CH
6	129.5, CH	130.0, CH	130.4, CH	128.7, CH	129.2, CH	128.9, CH	129.4, CH	125.2, CH
7	126.2, C	126.5, C	124.9, C	125.2, C	124.7, C	124.1, C	123.8, C	148.0, C
8	145.1, C	145.2, C	145.4, C	145.2, C	148.1, C	145.6, C	148.4, C	124.4, C
8a	127.4, C	125.4, C	126.6, C	126.6, C	126.2, C	127.0, C	126.6, C	131.3, C
9	168.2, CO	167.7, CO	167.8, CO	167.9, CO	167.3, CO	167.9, CO	167.3, CO	67.9, CH_2
10	104.8, CH	104.1, CH	104.4, CH	104.1, CH	97.0, CH	104.9, CH	97.2, CH	167.4, CO
4-$(CH_3)_2$	29.8, CH_3 29.7, CH_3	31.4, CH_3 30.2, CH_3	31.7, CH_3 29.6, CH_3	30.4, CH_3 30.3, CH_3	30.3, CH_3 30.2, CH_3	29.5, CH_3 29.2, CH_3	29.3, CH_3 29.2, CH_3	29.8, CH_3 29.8, CH_3
10-OCH_3	59.0, OCH_3	59.1, OCH_3	58.6, OCH_3	58.8, OCH_3		59.2, OCH_3		

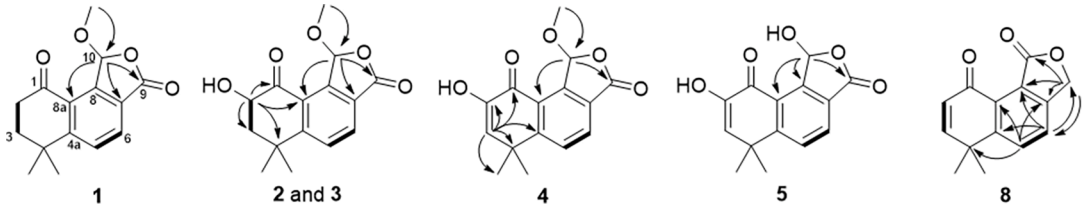

Fig. 2. Key HMBC (arrow) and COSY (bold) correlations (**1**–**5** and **8**).

$[M+H-I]^+$ and 226 $[M+H-I-OH]^+$ in **7** (Supporting Information S42 and S49). The experimental ECD spectra of **6** and **7** were in good agreement with the calculated spectra of the 10*S* models (Fig. 3). Based on the above information, the structures of **6** and **7**, designated as hyphodermins M and N, respectively, were established as shown.

Compound **8** was obtained as a white amorphous powder. The elemental composition of **8** was assigned as $C_{14}H_{12}O_3$ based on the HRESIMS analysis. The ^{1}H and ^{13}C NMR data exhibited that **8** had considerable similarity to 1-hydroxy-6,6-dimethyl-6H-naphtho[1,2-*c*]furan-3,9-(1*H*,6*H*)-dione (**11**) [8], except for the presence of a methylene group [δ_H 5.28 (2H, s, H-9)] at C-9 and a carbonyl group (δ_C 167.4) at C-10, as indicated by the HMBC and COSY correlations (Fig. 2). Therefore, the structure of compound **8** was elucidated as shown and has been assigned the trivial name hyphodermin O.

The known compounds were identified as hyphodermin B (**9**), 1-methoxy-6,6-dimethylnaphtho[1,2-*c*]furan-3,9(1*H*,6*H*)-dione (**10**), 1-hydroxy-6,6-dimethyl-6H-naphtho[1,2-*c*]furan-3,9-(1*H*,6*H*)-dione (**11**), 8-chloro-1-methoxy-6,6-dimethylnaphtho[1,2-*c*]furan-3,9(1*H*,6*H*)-dione (**12**), hyphodermin H (**13**), and hyphodermin C (**14**) based on the analyses of spectroscopic data of the NMR, MS, optical rotation, and ECD, and comparison with literature data [5–8].

All isolated compounds were assessed for their cytotoxicity on the DU-145 prostate cancer cells. Compounds **7**, **12**, **13**, and **14** reduced the viability of DU-145 cells (Supporting Information S64). Among the observed sample effects, compounds **7** and **14** strongly inhibited the proliferation of DU-145 cells with IC_{50} values of 7.54 ± 0.03 μM and 5.04 ± 0.03 μM (Supporting Information S65), respectively.

Then, the potential apoptotic cell death effects of compounds **7** and **14** were assessed on DU-145 cells using Alexa Fluor 488-conjugated annexin V. At a concentration of 8 μM, the fluorescence levels indicated by Annexin V labeling were higher in compound **7**- and **14**-treated groups than in the untreated group (Fig. 6A). Specifically, compounds **7** and **14** significantly increased the percentage of apoptotic cells to 15.30 ± 1.54% and 39.70 ± 1.19%, respectively, compared with 4.70 ± 0.27%

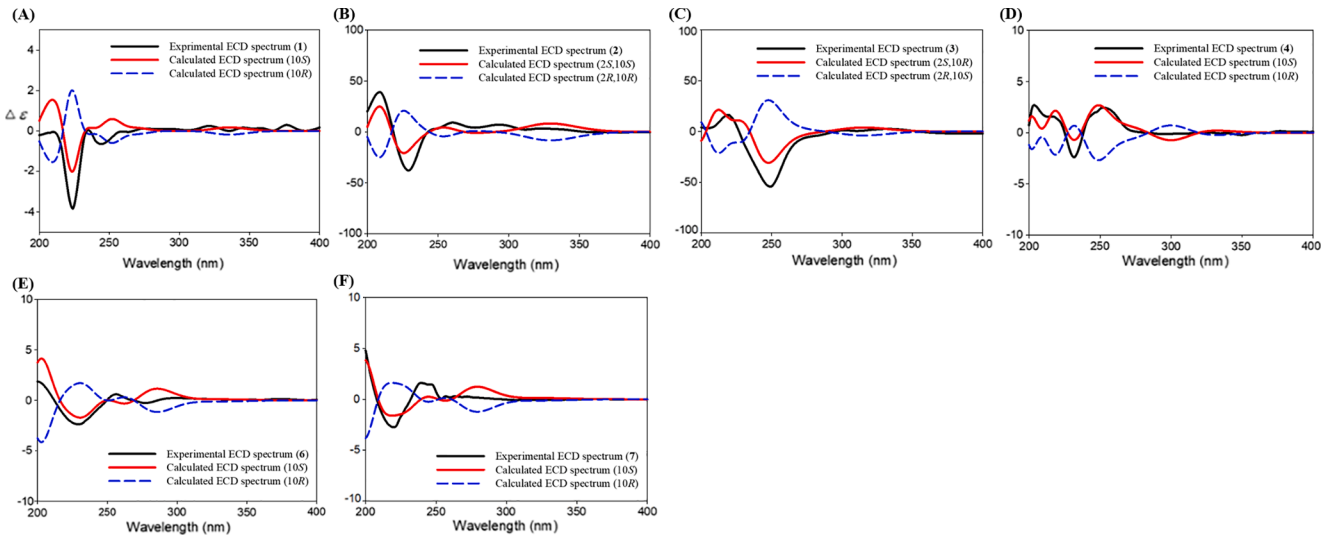

Fig. 3. Calculated and experimental ECD spectra of compounds **1** (A)–**4** (D), **6** (E), and **7** (F).

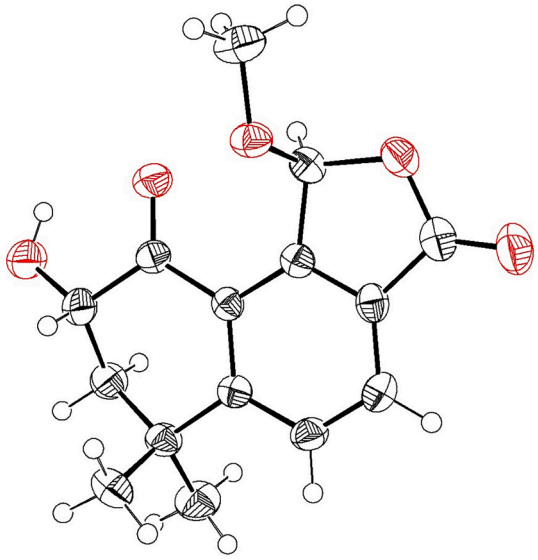

Fig. 4. X-ray ORTEP drawing of compound **2**.

in the control group (Fig. 6B). As previously reported, cisplatin induced apoptosis of cancer cells [28] and it was used as a positive control in the experiments. The results showed that cisplatin increased the percentage of apoptotic cells to 44.30 ± 1.66%. Based on the evidence that apoptosis is involved in the regulation of tumor adaptation to cancer treatment and cell death, the efficacy of most current clinical oncological treatments has been linked to induction of the apoptosis signal pathway [29]. Our results suggest that compounds **7** and **14** affect the death of DU-145 cells through the apoptosis pathways.

To elucidate the mechanism underlying the apoptosis-mediated death of DU-145 cells induced by compounds **7** and **14**, the protein expression of apoptosis-related pathways were evaluated using western blotting. After a 96-h treatment, compounds **7** and **14** upregulated the expression of cleaved forms of the caspase family proteins caspase 3, 7, 8, and 9 (Fig. 6C). Furthermore, cleaved-Poly (ADP-ribose) polymerase (PARP) and mitochondrial cytochrome *C* release were up-regulated in the compound-treated groups. However, full-length Bid was suppressed after 96-h of treatment. In most cases, anticancer chemotherapy usually results in activation of caspase proteins [30]. In the receptor-ligand mediator of caspase-dependent apoptosis, binding of anticancer drugs to the death receptor activates the initiator caspase 8, which can cleave itself [31]. Following activation, caspase 8 propagates the apoptosis signal by cleaving effector caspases of downstream activation such as caspase 3 and 7 [32]. Moreover, in mitochondrial mediators of caspase-

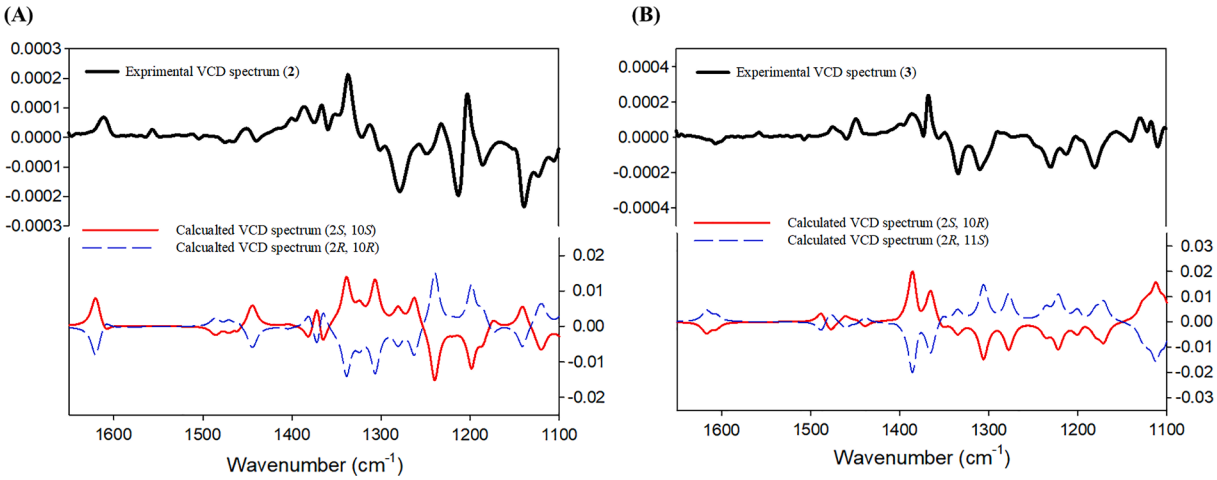

Fig. 5. Calculated and experimental VCD spectra of compounds **2** (A) and **3** (B).

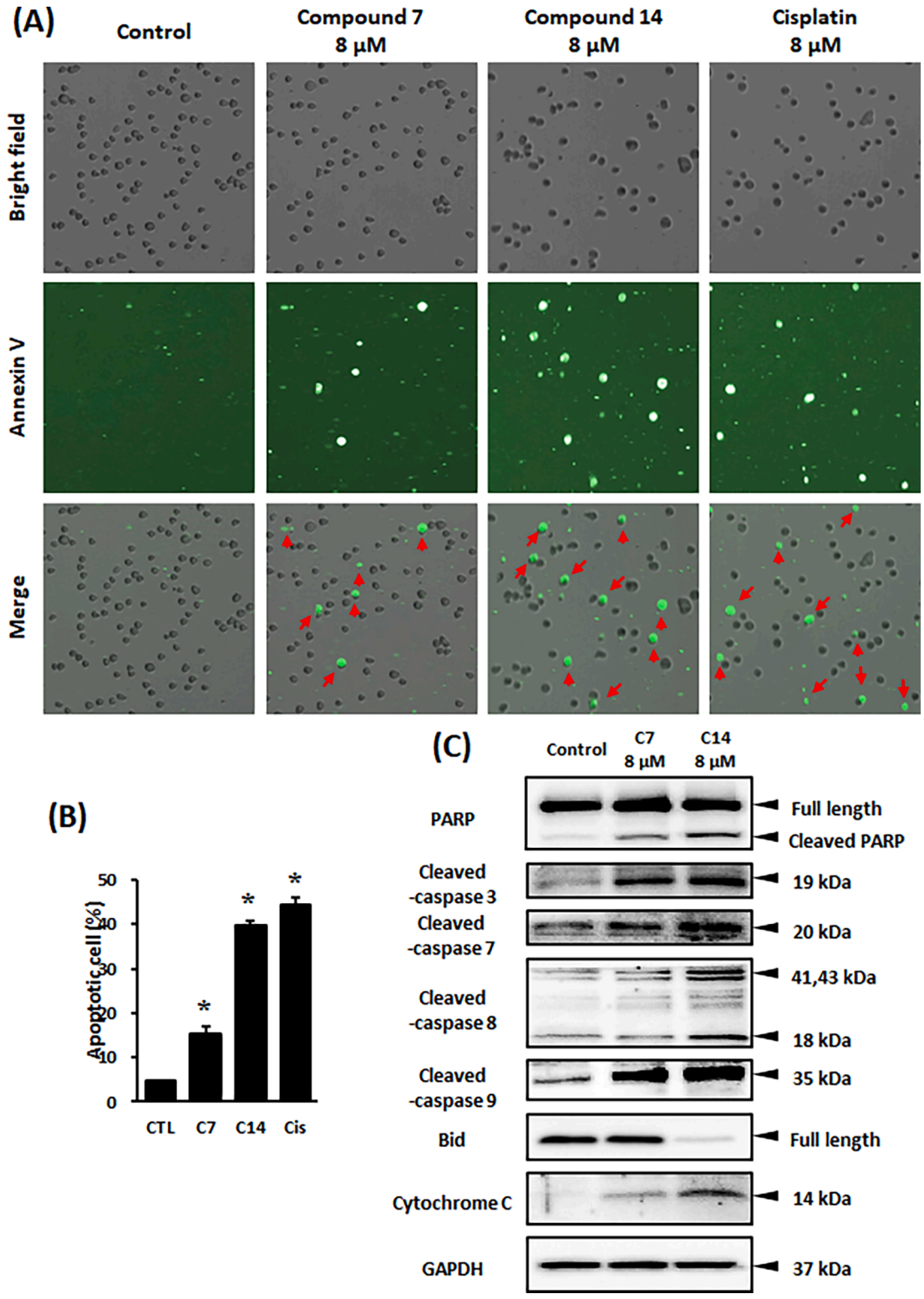

Fig. 6. (A, B) Compounds **7**- and **14**-induced apoptotic cell death and (C) expression of proteins related to the caspase-dependent apoptosis signaling pathway in DU-145 cells. Results are the mean ± SD. The difference in the mean values between groups was assessed using the Tukey method for one-way analysis of variance (ANOVA). *$p < 0.001$ versus the non-treated group. SD, standard deviation. Red arrows indicate apoptotic bodies. (For interpretation of the references to colour in this figure legend, the reader is referred to the web version of this article.)

dependent apoptosis, caspase 8 cleavage of Bid downregulates full-length Bid [33]. Then Bid activation results in regulating mitochondrial permeability and the cytochrome *C* release [34]. Cytochrome *C* induces activation of apoptosis-protease activating factor 1 (APAF1) which required for activating caspase 9 [35]. Next, caspase 9 cleavage downstream effector such as caspase 3,7 and PARP through a caspase 9-containing apoptosome complex [36]. Our result showed that compounds **7** and **14** may regulate apoptosis of DU-145 cells through both receptor-ligand and mitochondrial mediators of caspase-dependent apoptosis.

To obtain additional evidence of the regulation of DU-145 cell apoptosis by compounds **7** and **14**, a Hoechst assay of indicators of apoptotic cells was performed. After a 24-h treatment and staining with Hoechst dye, the fluorescence levels were increased to a greater extent in the compound- and cisplatin-treated groups than non-treated group (Fig. 7). These results indicate that compounds **7** and **14** induced chromatin condensation in DU-145 cells. Plasma membrane blebbing and morphological changes in the cells were observed under the bright field of the microscope. Nuclear fragmentation of the cells was observed in the compound- and cisplatin-treated groups (zoom images). Evidence of chromatin condensation, plasma membrane blebbing, and nuclear fragmentation are established hallmarks of apoptosis [37], and our data indicated that compounds **7** and **14** triggered these phenomena in DU-145 cells after a 24-h treatment.

To assess the effect of compound **7** and **14** on the immune cells, a proliferation assay of splenocytes isolated from cyclophosphamide-induce immunosuppressed mice was designed. After a 72-h treatment, no cytotoxicity on splenocytes was detected at the highest concentration of 20 μM compound treatment groups (Supporting Information S66). One of the disadvantages of chemotherapy is when reach the blood they both kill tumor cells and other cells, includes immune cells, without selectivity [38]. This is considered as the main reason for side effects of chemotherapy on normal tissues [39] and results in long-term immunosuppression of cancer patients [40] which increase the opportunistic diseases of patients [41]. Spleen is an immune organ that serves as a part of immune system [42]. Splenocytes include lymphocytes, macrophages, dendritic cells, plasma cells which play an essential role in immune reaction against pathology agents and cancer cells [43]. In this study, cyclophosphamide was used as an immunosuppression agent [44]. The data showed that to the concentration of 20 μM, compound **7** and **14** showed no effect on the proliferation of splenocytes isolated from immunosuppressed mice.

In conclusion, compounds **7** and **14** induced apoptosis of DU-145 cells through receptor-ligand and mitochondrial mediators of caspase-dependent apoptosis with evidence of microscopic morphological changes such as nuclear fragmentation, chromatin condensation, and plasma membrane blebbing. However, compound **7** and **14** exerted no effect on proliferation of splenocytes.

3. Conclusion

In summary, we described eight new naphtho[1,2-*c*]furan derivatives (**1**–**8**), together with six known compounds (**9**–**14**), from culture medium of the basidiomycete *Basidioradulum radula*. The chemical structures of the isolated compounds were identified using spectroscopic techniques, and all isolated compounds were evaluated for their cytotoxic effects on the DU-145 human prostate cancer cell line. Among them, compounds **7** and **14** strongly inhibited the proliferation of DU-145 cells without affecting proliferation of splenocytes. This study not only presented the new chemical constituents from *B. radula*, but also provided a potential candidate for the treatment of human prostate cancer.

4. Materials and methods

4.1. General experimental procedures

MPLC was run using a Biotage Isolera One system (Biotage AB, Uppsala, Sweden), and prep HPLC was performed using a Waters system (Waters, Milford, MA, USA) with a ODS-A column (250 × 20 mm i.d., 5 μm, YMC, Kyoto, Japan). NMR spectra were measured using a 500 MHz NMR spectrometer (Varian, Palo Alto, CA, USA). HRESIMS and MS/MS spectra were recorded using a Q-TOF Micromass spectrometer (Waters). UV and IR spectra were obtained using a UV–vis spectrophotometer (Mecasys, Daejeon, Korea) and 640 FT-IR spectrometer (Agilent, Palo Alto, CA, USA), respectively. Optical rotations were recorded using a P-2000 (Jasco, Tokyo, Japan). VCD and ECD spectra were recorded using a ChiralIR-2X TM FT-VCD spectrometer (BioTools, Jupiter, FL, USA) and a J-1100 spectrometer (Jasco). X-ray crystallography data were measured using a Bruker X-ray diffraction system (Bruker AXS GMBH, Karlsruhe, Germany).

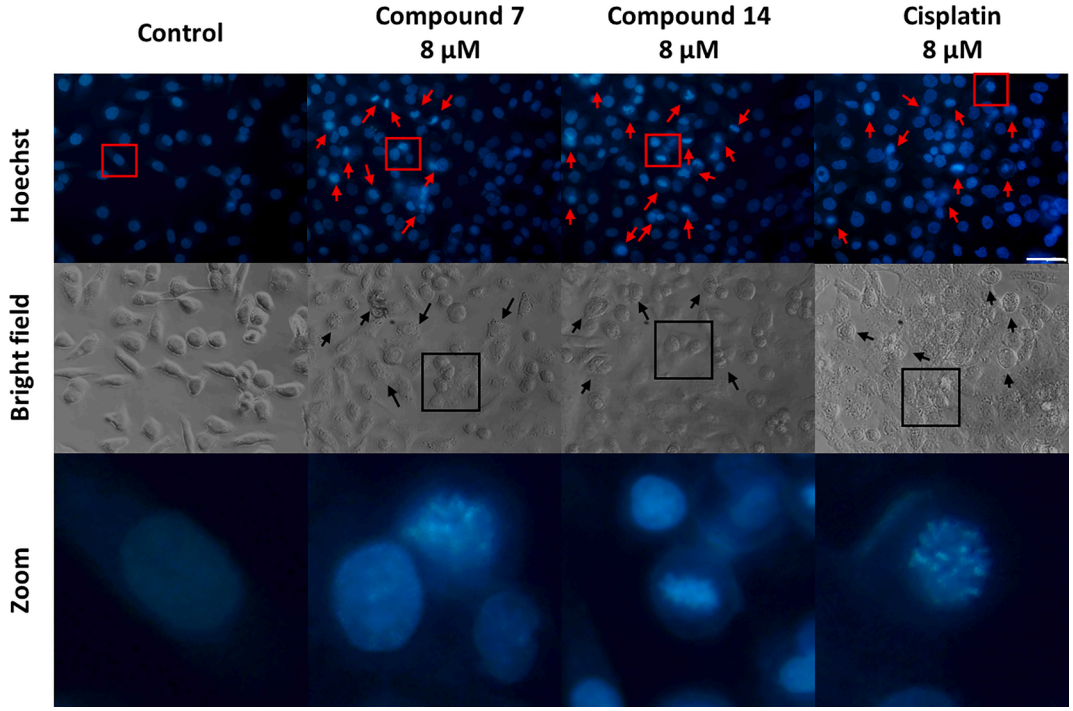

Fig. 7. Effect of compounds **7** and **14** on chromatin condensation of DU-145 cells (Scale bar is 100 μm). Red arrows indicate chromatin condensation cells. Black arrows and rectangle indicate plasma membrane blebbing. Red rectangles indicate chosen cells for zoom images. (For interpretation of the references to colour in this figure legend, the reader is referred to the web version of this article.)

4.2. Fungal material

B. radula was collected from Odaesan National Park, Republic of Korea in April 2013. A voucher specimen (KUC10671) was deposited at the Division of Environmental Science and Ecological Engineering, Korea University (Seoul, Korea). The strain was identified based on the molecular and phylogenetic analysis using large subunit ribosomal RNA regions and internal transcribed spacer (Supporting Information S67). All new sequences of *B. radula* KUC10671 were deposited in GenBank (accession no. ITS: MW575872, LSU: MW570869). *B. radula* was cultured on PDA culture medium in petri dishes (150 mm × 20 mm × 55 plates) at 25 °C for 30 days.

4.3. Extraction and isolation

The culture medium was extracted successively with MeOH (3 × 2.0 L) and EtOAc (3 × 2.0 L) to obtain the EtOAc-soluble extract (2.9 g). The extract was fractionated using MPLC with silica gel (*n*-hexane–$CHCl_3$–acetone = 1:1:0, 0:1:0 to 0:0:1, 30.0 mL/min) to afford 13 fractions (Fr 1–13). Fr 3 (88.0 mg) was purified using prep HPLC (MeCN–H_2O = 3:7 to 8:2, 8 mL/min) to yield compounds **1** (t_R 37.8 min, 9.4 mg), **6** (t_R 44.9 min, 4.7 mg), **12** (t_R 41.2 min, 39.6 mg), and **14** (t_R 33.7 min, 6.3 mg). Fr 4 (317.8 mg) was purified using MPLC with silica gel (*n*-hexane–EtOAc = 9:1 to 5:5, 20 mL/min) to obtain compounds **2** (148.1 mg), **3** (83.6 mg), and additional three sub-fractions (Fr 4.1–4.3). Fr 4.2 (38.3 mg) was purified using prep HPLC (MeCN–H_2O = 3:7 to 8:2, 8 mL/min) to obtain compounds **4** (t_R 28.6 min, 29.9 mg) and **10** (t_R 33.2 min, 6.2 mg). Fr 5 (185.3 mg) was purified using prep HPLC (MeCN–H_2O = 2:8 to 5:5, 8 mL/min) to yield compound **8** (t_R 26.5 min, 2.8 mg). Fr 6 (137.6 mg) was purified using prep HPLC (MeCN–H_2O = 3:7 to 6:4, 8 mL/min) to obtain compounds **7** (t_R 38.2 min, 4.8 mg), **9** (t_R 43.6 min, 6.8 mg), **11** (t_R 19.1 min, 35.7 mg), and **13** (t_R 35.5 min, 7.3 mg). Fr 9 (896.6 mg) was purified using prep HPLC (MeCN–H_2O = 2:8 to 5:5, 8 mL/min) to yield compound **5** (t_R 28.0 min, 14.5 mg).

*Hyphodermin I (**1**)*: white amorphous powder; $[\alpha]^{26}_D$ + 6.3 (*c* 0.01, MeOH); UV (MeOH) λ_{max} (log ε) 227 (3.96), 291 (2.90), 300 (2.92) nm; IR ν_{max} (ATR) 2962, 2932, 2864, 1773, 1689, 1606, 1472, 1444, 1365, 1330, 1283, 1237, 1130, 1067 cm^{-1}; ^1H and ^{13}C NMR (500 and 125 MHz, $CDCl_3$, Tables 1 and 2); ECD (*c* 0.2 mM, MeCN) $\Delta\varepsilon$ –6.1 (2 2 4); ESIMS (positive) *m/z* 261 $[M+H]^+$; HRESIMS *m/z* 261.1126 $[M+H]^+$ (calcd for $C_{15}H_{17}O_4$, 261.1127).

*Hyphodermin J (**2**)*: white amorphous powder; $[\alpha]^{26}_D$ + 166.1 (*c* 0.01, MeOH); UV (MeOH) λ_{max} (log ε) 224 (3.96), 290 (2.95), 298 (2.96) nm; IR ν_{max} (ATR) 3493, 2961, 2934, 1775, 1701, 1610, 1450, 1367, 1206, 1110, 1081, 1065, 1032 cm^{-1}; ^1H and ^{13}C NMR (500 and 125 MHz, $CDCl_3$, Tables 1 and 2); ECD (*c* 0.2 mM, MeCN) $\Delta\varepsilon$ + 66.3 (2 0 9), –67.7 (2 2 9); VCD (*c* 1.0 M, CDCl3, Fig. 4); ESIMS (positive) *m/z* 277 $[M+H]^+$; HRESIMS *m/z* 277.1085 $[M+H]^+$ (calcd for $C_{15}H_{17}O_5$, 277.1076).

*Isohyphodermin J (**3**)*: white amorphous powder; $[\alpha]^{26}_D$ –165.3 (*c* 0.01, MeOH); UV (MeOH) λ_{max} (log ε) 224 (3.96), 290 (2.95), 298 (2.96) nm; IR ν_{max} (ATR) 3489, 2965, 2936, 1773, 1699, 1607, 1451, 1367, 1205, 1107, 1067, 1029 cm^{-1}; ^1H and ^{13}C NMR (500 and 125 MHz, $CDCl_3$), Tables 1 and 2; ECD (*c* 0.2 mM, MeCN) $\Delta\varepsilon$ + 26.9 (2 2 0), –93.3 (2 4 8); VCD (*c* 1.0 M, CDCl3), Fig. 4; ESIMS (positive) *m/z* 277 $[M+H]^+$; HRESIMS *m/z* 277.1070 $[M+H]^+$ (calcd for $C_{15}H_{17}O_5$, 277.1076).

*Hyphodermin K (**4**)*: brown oil; $[\alpha]^{26}_D$ + 18.9 (*c* 0.01, MeOH); UV (MeOH) λ_{max} (log ε) 227 (3.96), 303 (3.50) nm; IR ν_{max} (ATR) 3398, 2970, 2935, 1775, 1652, 1611, 1455, 1404, 1364, 1313, 1260, 1205, 1157, 1123, 1087, 1046 cm^{-1}; ^1H and ^{13}C NMR (500 and 125 MHz, $CDCl_3$), Table 1 and 2; ECD (*c* 0.2 mM, MeCN) $\Delta\varepsilon$ –7.3 (2 3 1), +4.1 (2 5 6); ESIMS (positive) *m/z* 275 $[M+H]^+$; HRESIMS *m/z* 275.0907 $[M+H]^+$ (calcd for $C_{15}H_{15}O_5$, 275.0919).

*Hyphodermin L (**5**)*: brown oil; UV (MeOH) λ_{max} (log ε) 230 (3.94), 303 (3.61) nm; IR ν_{max} (ATR) 3397, 2971, 2934, 1763, 1650, 1610, 1445, 1404, 1364, 1312, 1261, 1205, 1133, 1088, 1049 cm^{-1}; ^1H and ^{13}C NMR (500 and 125 MHz, $CDCl_3$), Tables 1 and 2; ECD (*c* 0.2 mM, MeCN) $\Delta\varepsilon$ + 2.0 (2 0 8), –0.8 (2 1 4), +3.7 (2 2 6); ESIMS (positive) *m/z* 261 $[M+H]^+$; ESIMS (negative) *m/z* 259 $[M-H]^-$; HRESIMS *m/z* 261.0761 $[M+H]^+$ (calcd for $C_{14}H_{13}O_5$, 261.0763).

*Hyphodermin M (**6**)*: white amorphous powder; $[\alpha]^{26}_D$ + 14.0 (*c* 0.01, MeOH); UV (MeOH) λ_{max} (log ε) 229 (3.98), 300 (3.17) nm; IR ν_{max} (ATR) 2927, 2854, 1772, 1671, 1610, 1444, 1368, 1206, 1138, 1070 cm^{-1}; ^1H and ^{13}C NMR (500 and 125 MHz, $CDCl_3$), Tables 1 and 2; ECD (*c* 0.2 mM, MeCN) $\Delta\varepsilon$ –8.1 (2 3 4); ESIMS (positive) *m/z* 385 $[M+H]^+$; HRESIMS *m/z* 384.9923 $[M+H]^+$ (calcd for $C_{15}H_{14}IO_4$, 384.9937).

*Hyphodermin N (**7**)*: white amorphous powder; $[\alpha]^{26}_D$ + 4.9 (*c* 0.01, MeOH); UV (MeOH) λ_{max} (log ε) 230 (4.07), 301 (3.55) nm; IR ν_{max} (ATR) 3403, 2970, 2925, 2852, 1767, 1655, 1608, 1452, 1344, 1296, 1264, 1206, 1135, 1075, 1022 cm^{-1}; ^1H and ^{13}C NMR (500 and 125 MHz, $CDCl_3$), Tables 1 and 2; ECD (*c* 0.2 mM, MeCN) $\Delta\varepsilon$ –15.8 (2 2 8), +16.7 (2 3 4); ESIMS (positive) *m/z* 371 $[M+H]^+$; ESIMS (negative) *m/z* 369 $[M-H]^-$; HRESIMS *m/z* 370.9767 $[M+H]^+$ (calcd for $C_{14}H_{12}IO_4$, 370.9780).

*Hyphodermin O (**8**)*: white amorphous powder; UV (MeOH) λ_{max} (log ε) 221 (3.84), 255 (3.59) nm; IR ν_{max} (ATR) 2967, 2930, 2871, 1759, 1665, 1607, 1579, 1456, 1433, 1359, 1286, 1182, 1110, 1056, 1030 cm^{-1}; ^1H and ^{13}C NMR (500 and 125 MHz, $CDCl_3$), Tables 1 and 2; ESIMS (positive) *m/z* 229 $[M+H]^+$; HRESIMS *m/z* 229.0859 $[M+H]^+$ (calcd for $C_{14}H_{13}O_3$, 229.0865).

4.4. Computational methods

Conformer distributions, geometry optimizations, VCD, and ECD calculations of isolated compounds were conducted as described previously [45,46].

4.5. X-ray diffraction analysis

The crystal structure of **2** was determined using standard crystallographic methods. A colorless needlelike crystal was used for single-crystal X-ray diffraction. The data were recorded at 223(2) K using a Bruker D8 Venture equipped with an IμS micro-focus sealed tube Cu Kα (λ = 1.54178 Å) and a PHOTON III M14 detector in the Western Seoul Center of Korea Basic Science Institute. Data collection and integration were run using the SMART APEX3 software package (SAINT+) [47]. Absorption correction was carried out by the multi-scan method implemented in SADABS [48]. The chemical structure was refined using full-matrix least-squares with F2 using the SHELXTL program package [49]. Crystallographic data for **2** were deposited in the Cambridge Crystallographic Data Centre (CCDC 2031769).

*Crystallographic data of hyphodermin J (**2**)*: $C_{15}H_{16}O_5$, orthorhombic, M = 276.28, 0.321 × 0.218 × 0.123 mm^3, space group $P2_12_12_1$, a = 7.8659(5) Å, b = 12.2303(8) Å, c = 13.8787(10) Å, $\alpha = 90°$, $\beta = 90°$, $\gamma = 90°$, V = 1335.16(13) $Å^3$, Z = 4, μ = 0.863 mm^{-1}, T = 223(2) K, 14,017 reflection collected, 2762 independent reflections (R_{int} = 0.0260). The final R_1 values were 0.0290 [$I > 2\sigma(I)$] and the final wR^2 values were 0.0802 [$I > 2\sigma(I)$]. The goodness of fit on F^2 was 1.086. Absolute structure parameter = 0.07(4).

4.6. Cell culture

Human DU-145 prostate carcinoma cells (ATCC, Bethesda, MD, USA) were maintained in 10% fetal bovine serum-supplemented (FBS, Atlas Biologicals, Fort Collins, CO, USA) minimum essential medium (Gibco BRL, Carlsbad, MD, USA), added 100 Units/mL penicillin and 100 μMg/mL streptomycin (PS, Gibco BRL). The cells were cultured with 95% relative humidity, 5% CO_2, and 37 °C.

4.7. Cell proliferation assay

DU-145 cells were plated on 96-well plates at a density of 5 × 10^3 cells/well and incubated for 24-h. Following, the cells were treated with

several concentrations of the compounds for 96-h. The cells were supplemented with 10% of the Ez-Cytox cell proliferation assay kit (Daeil Lab Service Co., Seoul, Korea) in culture medium for 1-h. Cell proliferation was assessed by measuring the absorbance of samples at 450 nm using a microplate reader (PowerWave XS, Bio-Tek Instruments, Winooski, VT, USA).

4.8. Chromatin condensation

DU-145 cells were cultured on eight-well culture slides (SPL Life Sciences, Orlando, FL, USA) at a density of 5×10^4 cells/well for 24-h. Next, cells were incubated with samples for another 24-h. Then, the cells were stained with Hoechst 33,258 (Sigma-Aldrich, St. Louis, MO, USA) and observed under a fluorescence microscope (IX51, Olympus, Tokyo, Japan).

4.9. Apoptosis assay

DU-145 cells were plated on six-well plates at a density of 2.5×10^5 cells/well. After 24-h incubation, the cells were treated with the different concentrations of samples for 24-h. Next, the cells were harvested, and washed with Dulbecco's phosphate-buffered saline (DPBS, Welgene Inc., Daegu, Korea). This was followed by staining with Annexin V Alexa Fluor 488 (Invitrogen, Temecula, CA, USA) and dark adapted for 20 min. Bright field and fluorescence images were taken using a Tali image-based cytometer (Life Technologies Japan, Tokyo, Japan) and further analysis following manufacturer's instructions. The data were presented as the percentage of stained Annexin V cells dividing the total number of cells in each group.

4.10. Western blotting analysis

DU-145 cells were plated on 60 mm plates at a density of 4×10^5 cells/well for 24-h. Next, the cells were treated with the samples for 96-h and lysed in 1 × RIPA buffer (Tech & Innovation, Gangwon, Korea) supplemented with a proteinase inhibitor cocktail (Roche Diagnostics, Basel, Switzerland) to harvest whole-cell extracts. Extraction of proteins from cells in each sample suspension were measured using the Pierce BCA protein assay kit (Thermo Fisher Scientific, Waltham, MA, USA). A same amount of protein mixture is separated using electrophoresis of 15% sodium dodecyl sulfate–polyacrylamide gel and transferred onto polyvinylidene difluoride membranes. Next, the membranes were blocked with 5% skim milk in Tris-buffered saline (1 ×) at 4 °C overnight, and the separated proteins were identified by incubation with epitope-specific primary and secondary antibodies (Cell Signaling Technology, Danvers, MA, USA). The membranes were visualized using SuperSignal West Femto Maximum Sensitivity Substrate (Thermo Fisher Scientific) and captured using a FUSION Solo Chemiluminescence System (Vilber Lourmat Deutschland GmbH, Eberhardzell, Germany).

4.11. Proliferation assay of splenocytes isolated from cyclophosphamide-induce immunosuppressed mice

Four six-week-old C57BL/6 mice were induced immunosuppression by injection of 100 mg/kg cyclophosphamide (Thermo Fisher Scientific) at the day 18 and 150 mg/kg cyclophosphamide at day 16 before sacrifice. The spleens were harvested and washed with DPBS supplemented with 1% penicillin (Gibco BRL). Then, the spleens were homogenized and suspended in 10% FBS-supplemented (Atlas Biologicals) RPMI GlutaMAX medium (Gibco BRL), supplemented 100 Units/mL penicillin and 100 μg/mL streptomycin (Gibco BRL). Red blood cells were lysed with lysis buffer (Sigma-Aldrich). The cells were cultured with 95% relative humidity, 5% CO_2, and 37 °C in an incubator. Splenocyte cells were plated on a 96 well-plate with the density of 4×10^5 cells/well and treated with different concentrations of the compounds for 72-h. Next, the cells were supplemented with 10% of the Ez-Cytox cell proliferation assay kit (Daeil Lab Service Co.) in culture medium for 1-h. Cell proliferation was evaluated by measuring the optical density of samples at 450 nm using a microplate reader (PowerWave XS, Bio-Tek Instruments).

4.12. Data analysis

Cell experiments were conducted at least in triplicate. The results are presented as the means ± standard error of mean (SEM). The significance results of mean values were evaluated by one-way analysis of variance (ANOVA) and followed by a Tukey's honestly significant difference (HSD) test using R program (version 3.3.3). IC_{50} was evaluated by GraphPad Prism version 7.04.

Declaration of Competing Interest

The authors declare that they have no known competing financial interests or personal relationships that could have appeared to influence the work reported in this paper.

Acknowledgements

This research was supported by the Korea University, the National Research Foundation of Korea (Grants: NRF-2019R1A2C1006226 and NRF-2019R1A4A1020626), and Korea Polar Research Institute (Grant: PE21150).

Appendix A. Supplementary material

Supplementary data to this article can be found online at https://doi.org/10.1016/j.bioorg.2021.105064.

References

[1] M.K. Nobles, Conspecificity of *Basidioradulum (Radulum) radula* and *Corticium hydnans*, Mycologia 59 (2) (1967) 192–211.
[2] Y. Jang, S. Jang, J. Lee, H. Lee, Y.W. Lim, C. Kim, J.-J. Kim, Diversity of wood-inhabiting polyporoid and corticioid fungi in Odaesan National Park, Korea, Mycobiology 44 (4) (2016) 217–236.
[3] W. Xue-Wei, J. Ji-Hang, Z. Li-Wei, Basidioradulum mayi and B. tasmanicum spp. nov.(Hymenochaetales, Basidiomycota) from both sides of Bass Strait, Australia, Sci. Rep. 10(1) (2020) 1-9.
[4] E. Yurchenko, J. Riebesehl, E. Langer, Fasciodontia gen. nov.(Hymenochaetales, Basidiomycota) and the taxonomic status of Deviodontia, Mycol. Prog. 19(2) (2020) 171-184.
[5] H.M. Thomas H., Delf S., Hartmund W., D.E. Patent 19611366A1, 1997.
[6] W.A. Loughlin, G.K. Pierens, M.J. Petersson, L.C. Henderson, P.C. Healy, Evaluation of novel hyphodermin derivatives as glycogen phosphorylase a inhibitors, Bioorg. Med. Chem. 16 (11) (2008) 6172–6178.
[7] L.C. Henderson, W.A. Loughlin, I.D. Jenkins, P.C. Healy, M.R. Campitelli, Efficient formal synthesis of (±)-hyphodermin B, J. Org. Chem. 71 (6) (2006) 2384–2388.
[8] W.A. Loughlin, I.D. Jenkins, L.C. Henderson, M.R. Campitelli, P.C. Healy, Total synthesis of (±)-Hyphodermins A and D, J. Org. Chem. 73 (9) (2008) 3435–3440.
[9] K.-L. Lin, J.-C. Su, C.-M. Chien, C.-H. Tseng, Y.-L. Chen, L.-S. Chang, S.-R. Lin, Naphtho[1,2-*b*]furan-4,5-dione disrupts Janus kinase-2 and induces apoptosis in breast cancer MDA-MB-231 cells, Toxicol. In Vitro 24 (4) (2010) 1158–1167.
[10] J.-C. Su, K.-L. Lin, C.-M. Chien, C.-H. Tseng, Y.-L. Chen, L.-S. Chang, S.-R. Lin, Naphtho[1,2-*b*]furan-4,5-dione inactivates EGFR and PI3K/Akt signaling pathways in human lung adenocarcinoma A549 cells, Life Sci. 86 (5–6) (2010) 207–213.
[11] C.-Y. Hsieh, P.-C. Tsai, C.-H. Tseng, Y.-L. Chen, L.-S. Chang, S.-R. Lin, Inhibition of EGF/EGFR activation with naphtho[1,2-*b*]furan-4,5-dione blocks migration and invasion of MDA-MB-231 cells, Toxicol. In Vitro 27 (1) (2013) 1–10.
[12] P.-C. Tsai, C.-L. Chu, Y.-S. Fu, C.-H. Tseng, Y.-L. Chen, L.-S. Chang, S.-R. Lin, Naphtho[1,2-*b*]furan-4,5-dione inhibits MDA-MB-231 cell migration and invasion by suppressing Src-mediated signaling pathways, Mol. Cell. Biochem. 387 (1) (2014) 101–111.
[13] P.C. Tsai, C.L. Chu, C.H. Tseng, Y.l. Chen, L.S. Chang, S.R. Lin, Inhibitory action of naphtho[1,2-b]furan-4,5-dione on hepatocyte growth factor-induced migration and invasion of MDA-MB-231 cells: Mechanisms of action, Clin. Exp. Pharmacol. Physiol. 41(9) (2014) 716-726.
[14] R. Hodson, Small organ, big reach, Nature 528 (7582) (2015) 118–119.
[15] A. Law, D. McLaren, Non-surgical treatment for early prostate cancer, J. R. Coll. Physicians Edinb. 40 (4) (2010) 340–342.
[16] N. Lawrentschuk, G. Trottier, C. Kuk, A. Zlotta, Role of surgery in high-risk localized prostate cancer, Curr. Oncol. 17 (Suppl 2) (2010) 25–32.

[17] C. O'Hanlon Brown, J. Waxman, Current management of prostate cancer: dilemmas and trials, Br. J. Radiol. 85 (special_issue_1) (2012) 28–40.
[18] N.M. Hoosein, D.D. Boyd, W.J. Hollas, A. Mazar, J. Henkin, L.W. Chung, Involvement of urokinase and its receptor in the invasiveness of human prostatic carcinoma cell lines, Cancer Commun. 3 (8) (1991) 255–264.
[19] M.E. Laniado, E.-N. Lalani, S.P. Fraser, J.A. Grimes, G. Bhangal, M. Djamgoz, P. D. Abel, Expression and functional analysis of voltage-activated Na+ channels in human prostate cancer cell lines and their contribution to invasion *in vitro*, Am. J. Pathol. 150 (4) (1997) 1213–1221.
[20] F. Alimirah, J. Chen, Z. Basrawala, H. Xin, D. Choubey, DU-145 and PC-3 human prostate cancer cell lines express androgen receptor: implications for the androgen receptor functions and regulation, FEBS Lett. 580 (9) (2006) 2294–2300.
[21] K. Minamiguchi, M. Kawada, T. Someno, M. Ishizuka, Androgen-independent prostate cancer DU145 cells suppress androgen-dependent growth of prostate stromal cells through production of inhibitory factors for androgen responsiveness, Biochem. Biophys. Res. Commun. 306 (3) (2003) 629–636.
[22] S. Howell, Resistance to apoptosis in prostate cancer cells, Mol. Urol. 4 (3) (2000) 225–229.
[23] P. Hemmati, D. Güner, B. Gillissen, J. Wendt, C. Von Haefen, G. Chinnadurai, B. Dörken, P. Daniel, Bak functionally complements for loss of Bax during p14 ARF-induced mitochondrial apoptosis in human cancer cells, Oncogene 25 (50) (2006) 6582–6594.
[24] J.W. Ha, J. Kim, H. Kim, W. Jang, K.H. Kim, Mushrooms: An Important Source of Natural Bioactive Compounds, Nat. Prod. Sci. 26 (2) (2020) 118–131.
[25] C. Lee, S.H. Shim, Endophytic Fungi Inhabiting Medicinal Plants and Their Bioactive Secondary Metabolites, Nat. Prod. Sci. 26 (1) (2020) 10–27.
[26] L.M. Kutrzeba, D. Ferreira, J.K. Zjawiony, Salvinorins J from Salvia divinorum: mutarotation in the neoclerodane system, J. Nat. Prod. 72 (7) (2009) 1361–1363.
[27] I. Liblikas, E.M. Santangelo, J. Sandell, P. Baeckström, M. Svensson, U. Jacobsson, C.R. Unelius, Simplified isolation procedure and interconversion of the diastereomers of nepetalactone and nepetalactol, J. Nat. Prod. 68 (6) (2005) 886–890.
[28] Z.H. Siddik, Cisplatin: mode of cytotoxic action and molecular basis of resistance, Oncogene 22 (47) (2003) 7265–7279.
[29] S. Fulda, K.-M. Debatin, Extrinsic versus intrinsic apoptosis pathways in anticancer chemotherapy, Oncogene 25 (34) (2006) 4798–4811.
[30] M.O. Hengartner, The biochemistry of apoptosis, Nature 407 (6805) (2000) 770–776.
[31] D.R. Green, F. Llambi, Cell death signaling, Cold Spring Harb. Perspect. Biol. 7 (12) (2015) 1–24.
[32] A. Clark, S.H. MacKenzie, Targeting cell death in tumors by activating caspases, Curr. Cancer Drug Targets 8 (2) (2008) 98–109.
[33] Z.T. Schug, F. Gonzalvez, R. Houtkooper, F.M. Vaz, E. Gottlieb, BID is cleaved by caspase-8 within a native complex on the mitochondrial membrane, Cell Death Differ. 18 (3) (2011) 538–548.
[34] X. Luo, I. Budihardjo, H. Zou, C. Slaughter, X. Wang, Bid, a Bcl2 interacting protein, mediates cytochrome c release from mitochondria in response to activation of cell surface death receptors, Cell 94 (4) (1998) 481–490.
[35] C. Garrido, L. Galluzzi, M. Brunet, P. Puig, C. Didelot, G. Kroemer, Mechanisms of cytochrome c release from mitochondria, Cell Death Differ. 13 (9) (2006) 1423–1433.
[36] D.R. McIlwain, T. Berger, T.W. Mak, Caspase functions in cell death and disease, Cold Spring Harbor Perspect. Biol. 5 (a008656) (2013) 1–28.
[37] D.T. Loo, J.R. Rillema, Measurement of Cell Death, Methods Cell Biol. 57 (1998) 251–264.
[38] L. Zitvogel, L. Apetoh, F. Ghiringhelli, G. Kroemer, Immunological aspects of cancer chemotherapy, Nat. Rev. Immunol. 8 (1) (2008) 59–73.
[39] A. Coates, S. Abraham, S.B. Kaye, T. Sowerbutts, C. Frewin, R. Fox, M. Tattersall, On the receiving end—patient perception of the side-effects of cancer chemotherapy, Eur. J. Cancer Clin. Oncol. 19 (2) (1983) 203–208.
[40] G.T. Kovacs, O. Barany, B. Schlick, M. Csoka, J. Gado, A. Ponyi, J. Müller, J. Nemeth, P. Hauser, D.J. Erdelyi, Late immune recovery in children treated for malignant diseases, Pathol. Oncol. Res. 14 (4) (2008) 391–397.
[41] S. Vento, F. Cainelli, Infections in patients with cancer undergoing chemotherapy: aetiology, prevention, and treatment, Lancet Oncol. 4 (10) (2003) 595–604.
[42] M.F. Cesta, Normal structure, function, and histology of the spleen, Toxicol. Pathol. 34 (5) (2006) 455–465.
[43] J.M. Den Haan, R. Mebius, G. Kraal, Stromal cells of the mouse spleen, Front. Immunol. 3 (2012) 201–205.
[44] M. Ahlmann, G. Hempel, The effect of cyclophosphamide on the immune system: implications for clinical cancer therapy, Cancer Chemother. Pharmacol. 78 (4) (2016) 661–671.
[45] J. Kwon, Y.H. Seo, J.-E. Lee, E.-K. Seo, S. Li, Y. Guo, S.-B. Hong, S.-Y. Park, D. Lee, Spiroindole alkaloids and spiroditerpenoids from *Aspergillus duricaulis* and their potential neuroprotective effects, J. Nat. Prod. 78 (11) (2015) 2572–2579.
[46] S.M. Ryu, H.M. Lee, E.G. Song, Y.H. Seo, J. Lee, Y. Guo, B.S. Kim, J.-J. Kim, J. S. Hong, K.H. Ryu, D. Lee, Antiviral activities of trichothecenes isolated from *Trichoderma albolutescens* against *pepper mottle virus*, J. Agric. Food Chem. 65 (21) (2017) 4273–4279.
[47] SMART, SAIT and SADABS, Bruker AXS Inc., Madision, WI, USA, 2016.
[48] SADABS, University of Göttingen, Göttingen, Germany, 2002.
[49] SHELXTL, Bruker AXS, Inc, Wisconsin, USA, 2000.